THE JOURNAL OF PHYSICAL CHEMISTRY C

Article

pubs.acs.org/JPCC

Impedance Spectroscopy Analysis of the Effect of TiO_2 Blocking Layers on the Efficiency of Dye Sensitized Solar Cells

Márcio Sousa Góes,*[,†] Ednan Joanni,[‡] Elaine C. Muniz,[†] Raluca Savu,[§] Thomas R. Habeck,[†] Paulo R. Bueno,[†] and Francisco Fabregat-Santiago*[,∥]

[†]Instituto de Química, Depto. Físico-Química, Universidade Estadual Paulista - UNESP, R. Prof. Francisco Degni, n. 55, 14800-900, Araraquara SP, Brazil

[‡]Centro de Tecnologia da Informação Renato Archer (CTI), Rod. Dom Pedro I km 143.6, 13069-901, Campinas, SP, Brazil

[§]Centro de Componentes Semicondutores - CCS, Universidade de Campinas - UNICAMP, C.P. 6061, Rua João Pandia Calógeras, 90, 13083-870, Campinas, SP, Brazil

[∥]Grup de Dispositius Fotovotaics i Optoelectrònics, Departament de Física, Universitat Jaume I, Av. SosBaynat, s/n, 12071, Castelló de la Plana, Spain

Supporting Information

ABSTRACT: The introduction of a dense TiO_2 layer between the mesoporous TiO_2 network and the charge collector in dye-sensitized solar cell anodes has been claimed to improve the performance of solar cell devices. Two mechanisms have been proposed to explain this behavior, a decrease in the electron−hole recombination at substrate/electrolyte interface and an enhancement in the electronic contact between the mesoporous TiO_2 network and the charge collecting electrode. In this work the effect of sputtered TiO_2 blocking layers (BLs) on the performance of dye-sensitized solar cells electrodes has been analyzed. It has been shown that the electron injection efficiency governed changes observed in cell efficiency. The thicker the BL, the poorer the photocurrent, and therefore, only thin BLs leaded to an increase in energy conversion efficiencies. The thickness of the BL also affected the internal series resistance of the solar cells, influencing their fill factor.

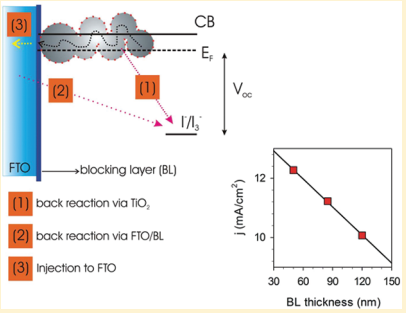

1. INTRODUCTION

Dye-sensitized solar cells[1] have been the focus of intense research worldwide, mainly due to their potential as low cost energy production technology.[2,3] Up to now, the highest energy conversion efficiencies reported for DSCs are around 11−12%.[4−6] Many variants for these devices are being explored with the aim of increasing their performance to compete with conventional silicon-based solar cells (p−n junctions).[7]

A great deal of this research has been focused on the optimization of the device performance after understanding the mechanisms responsible for the efficiency losses. The main back-reactions limiting the photocurrent and photopotential of the cell are: radiationless relaxation of the excited state of the dye, recombination of the electrons with the oxidized dye and electron recombination with the tri-iodide in the electrolyte.[8−10] In high performance DSCs, the first two mechanisms have little impact, with the TiO_2/electrolyte and electrode/electrolyte interfaces being responsible for most of the electron losses. These interface losses and the mismatches between the energy levels of the different components of the device impose the limits on the maximum achievable photopotential and photocurrent.[11] Further performance losses, affecting the fill factor, are associated to the presence of series resistances in the cell.[12,13]

At the point of maximum power efficiency of DSCs, electron recombination losses are generally greater in the bulk of the sensitized layer than close to the FTO substrate.[8,14] However, under short circuit conditions, the TiO_2 conduction band is far from the Fermi level while in the FTO it is aligned with the redox Fermi level, yielding a recombination governed by the FTO/electrolyte interface rather than by TiO_2.[8,14,15] Therefore, to obtain high efficiency devices, both routes of interface recombination, TiO_2/electrolyte and FTO/electrolyte, need to be optimized to prevent the loss of electrons by back reactions.

The application of barrier layers at these interfaces has been proposed as a viable approach toward this goal. These barrier layers can be dense films at the FTO surface (the "blocking layer" or BL)[14−16] or a thin layer over the TiO_2 nanoparticles (the so-called "core-shell" configuration).[17−19] Recent research in the use of BLs coating the FTO substrate and interfacing it with the nanostructured TiO_2 matrix has shown improvements in the overall conversion efficiency of DSCs.[20−22]

In the present work we investigate the effect of the thickness of sputtered TiO_2 BLs in the performance of DSCs. These layers were either obtained *in situ* from an oxide target or by

Received: February 21, 2012
Revised: May 14, 2012
Published: May 21, 2012

deposition using a metal target followed by heat treatment in air. The electron recombination and accumulation at the interfaces were analyzed by impedance spectroscopy (IS). This technique has been proved to be very powerful to discriminate the charge transfer processes in the different interfaces of the DSCs.[23,24] We observed clear performance improvements for some of the applied barrier layers. A strong dependence of photocurrent on BL thickness was found which limits the size of BL to be used in DSCs.

2. EXPERIMENTAL DETAILS

2.1. Deposition of Blocking Layers. The TiO_2 and Ti films were deposited using radio frequency (RF) and direct current (DC) sputtering, respectively. In both cases, borosilicate glass substrates covered with a layer of about 500 nm FTO (Solaronix 10 $\Omega\square^{-1}$, 5 cm^2) were used. After cleaning the substrates with isopropyl alcohol, the layers were deposited using shadow masks placed on one edge of each substrate, preventing the deposition of material in these regions and allowing the electrodes to remain exposed for the electrical measurements. Before the onset of film deposition, the chamber was evacuated to pressures below 10^{-5} Torr. All depositions were carried out in 2×10^{-2} Torr argon using 150 W sputtering power and 2 inch diameter targets. The TiO_2 layers were either obtained directly from oxide targets or indirectly, using Ti targets followed by thermal treatment in air (during the subsequent treatment of the mesoporous TiO_2 deposit). The deposition rate was 0.9 Å·s^{-1} for the TiO_2 layers and 0.2 Å·s^{-1} for the Ti films. The oxide layers (henceforth called *oxide series*, OS) were deposited with thicknesses of 50, 85, and 120 nm, while the titanium films (called *metallic series*, MS) had thicknesses of 40, 70, and 100 nm. The different electrodes studied and their nomenclatures are summarized in Table 1. To have all of the samples with approximately the same thicknesses, the metal films were made thinner, taking into account the subsequent volume increase during oxidation.

Table 1. Thickness and Materials Deposited on FTO for Building the Blocking Layers

series	sample code	material	layer thickness (nm)
oxide	TO5	TiO_2	50
	TO8	TiO_2	85
	TO12	TiO_2	120
metallic	T4	Ti	40
	T7	Ti	70
	T10	Ti	100
bare FTO	F		

2.2. DSC Fabrication. All DSCs in this work were fabricated using a TiO_2 paste from Dyesol (DSL-90-T). The paste was applied by doctor blade on the substrates prepared by sputtering (uncoated FTO substrates were used as reference/standard) and sintered in air at 450 °C for 30 min. The metallic Ti films were oxidized to TiO_2 during this heat treatment, and the mesoporous films obtained through this process had a thickness between 7.5 and 8.0 μm and an active area of 0.36 cm^2. After cooling to 80 °C, the TiO_2 electrodes were immersed for 15 h in a 0.5 mmol·L^{-1} *cis*-bis(isothiocyanato)-bis(2,2′-bipyridyl-4,4′-dicarboxylato)-Ru(II) (N3, Solaronix) solution in absolute ethanol. The iodide-based redox shuttle solution (50 mmol·L^{-1} of tri-iodide in acetonitrile, Iodolyte AN-50, Solaronix) was dripped between the FTO/TiO_2/dye working electrode and the Pt-coated FTO-glass counter-electrode. The counter-electrode was prepared by deposition of Pt onto FTO-coated glass (Xopglass, 8 $\Omega\square^{-1}$) via thermal decomposition of H_2PtCl_6 solution (2 mg of Pt in 1 mL of ethanol) at 450 °C for 30 min. The dye-covered TiO_2 electrodes and Pt counter electrodes were assembled into a sandwich-type cell and sealed with a Surlyn 1702 hotmelt gasket 50 μm thick. Finally, the assembled cell was filled with the electrolyte containing the I^-/I_3^- redox couple.

2.3. Characterization. Current−voltage ($j-V$), cyclic voltammetry (CV) and IS measurements were performed both in two- and three-electrode configurations. The electrochemical experiments were conducted using a three-electrode configuration with Ag/AgCl (3 mol·L^{-1} in KCl) as a reference, platinum as a counter electrode, and FTO with and without BLs as working electrodes. These samples were not loaded with the nanocolloidal TiO_2, thus having the optimal configuration FTO/BL for analyzing the processes occurring at the substrate/electrolyte interface. The samples were called T and TO, denoting the metallic series and oxide series, respectively, as indicated in Table 1. The CV was performed at the scan rate of 10 mV·s^{-1}, and the IS measurements were recorded (Autolab PGSTAT30) over a frequency range of 5 mHz to 400 kHz with an AC amplitude of 20 mV in the range between 0 and −0.8 V with steps of 50 mV. The electrolyte used in these experiments was Iodolyte AN-50 (Solaronix).

For two electrode measurements, complete devices prepared with the different substrates were called DT and DTO, to denote the cells built from metallic and oxide series substrates, respectively. Impedance measurements were carried out under different bias potentials (in the range between 0 and −0.85 V) in the dark and under illumination (1 sun, AM1.5 solar radiation). For the photovoltaic measurements, the DSCs were illuminated with an AM1.5 solar light simulator (SolarLight XPS400) at 100 mW·cm^{-2}, and their current density−voltage ($j-V$) characteristics were registered with a Solartron 1287 potentiostat/galvanostat. Electrochemical characterization (CV and IS) was performed with a Solartron 1260 impedance/gain-phase analyzer. The amplitude of the AC signal used in IS was 20 mV, and the frequency was varied between 10 mHz and 1 MHz.

The Zview equivalent circuit modeling software was employed for data fitting, using a built-in extended element or RC circuit. A Varian Cary 300 Bio UV−vis spectrophotometer was used to obtain the transmittance spectra, in the range from 200 to 800 nm, of the FTO substrates with and without BLs.

3. RESULTS AND DISCUSSION

3.1. Electrochemical Analysis (Three-Electrode Configuration). The first step in this study is the analysis of the effect of the BLs over the FTO substrate in the absence of the TiO_2 mesoporous matrix and sensitizer. The IS measurements of the FTO substrates with and without BLs, immersed in a solution containing the I^-/I_3^- redox couple, were performed at potentials ranging from 0.15 to −0.7 V versus I^-/I_3^- redox couple, using a three-electrode configuration. These values were obtained taking iodide−triiodide as a reference with formal potential of +0.35 V versus a normal hydrogen electrode (NHE).[22] Note that small variations from formal potential due to the difference in concentration between iodide and triiodide may produce. This shift was estimated to be lower than 20 mV using the Nernst equation. Representative spectra obtained at

−0.1 V are shown in Figure 1. From the two arcs appearing in the spectra, the most important contribution is a large low

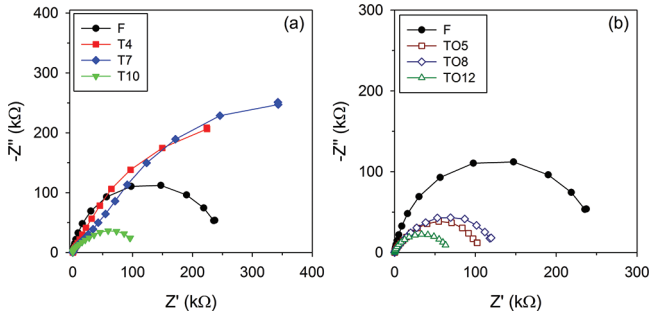

Figure 1. Impedance spectra for the different substrates measured at −0.1 V applied potential, using a three-electrode configuration: (a) MS and (b) OS.

frequency semicircle, which corresponds to electron transfer at the substrate/electrolyte interface.

Figure 2 shows the results of capacitance and charge transfer resistance values for FTO with and without BLs, obtained from

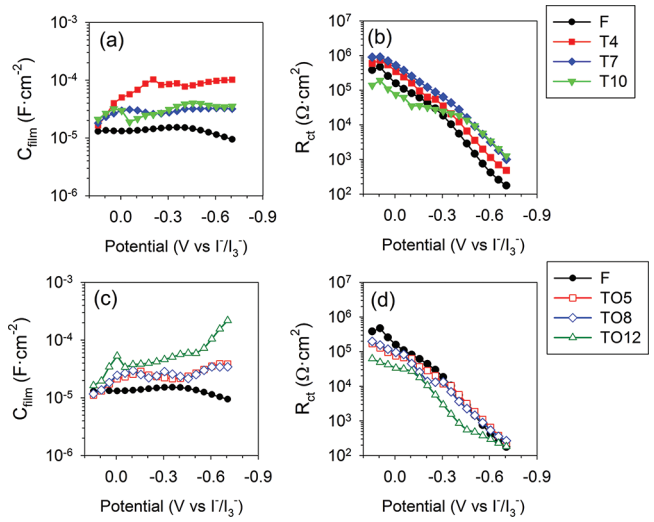

Figure 2. Capacitance (a, c) and the charge transference resistance (b, d) of bare or BL coated FTO measured in a three-electrode configuration.

the fittings of impedance data at all of the potentials measured. The measured capacitance (Figures 2a,c) is attributed to the charge accumulation at the electrode surface. In the bare FTO sample, the value of capacitance, near 10 μF·cm^{-2}, is due to the Helmholtz layer at the surface of the electrode combined with the depletion layer of the highly doped FTO. The higher capacitance values observed for both MS and OS samples suggest that the BL is not just behaving as a simple dielectric. If this were the case, given the dimensions of the layer, the result would have been a reduction in the overall measured capacitance.[25] Instead data suggest that the BL presents a high enough conductivity to allow a strong influence of the Helmholtz layer in the total capacitance of the electrolyte. In this situation, the increase in the value of film capacitance (C_{film}) indicates an increase of the effective surface area of electrode in contact with the electrolyte for the cells with BL or, in other words, that the films is somewhat porous.

Charge transference resistance (in this case, recombination resistance) data presented in Figure 2b,d confirm the film's porosity. In the samples with larger capacitance (T4 for MS and TO12 for OS) present the lowest charge transference resistances (R_{ct}) of their series, while both T7 and T10 (at high potentials) for MS and TO5 and TO8 for OS showed similar recombination resistances and the same capacitances. When compared to FTO (black curve), OS samples present lower R_{ct}, while MS samples exhibit larger values. These differences may be attributed to the different methods of preparation of the BLs and the different charge transfer mechanisms of FTO and TiO_2. Therefore, it appears that the metallic films can be more effective as BLs than the ones from the oxide series.

Data from cyclic voltammetry performed without illumination in Figure 3 show similar trends as for the impedance

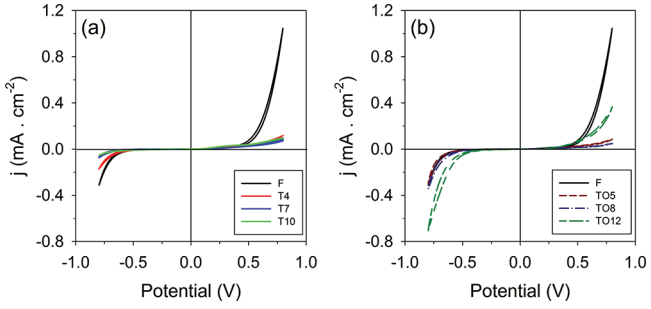

Figure 3. CV curves, performed in a three-electrode configuration, for substrates with and without BLs: MS (a) and OS (b).

measurements. At negative potentials, the current of MS is smaller than the ones for uncoated FTO (F) and OS samples. This result reflects that the order in the reduction of the dark current at the working (negative) potentials is MS > F > OS, although the importance of this aspect is small since the absolute values of R_{ct} are large. Contrarily, at positive potentials, except for TO12 sample, the current of OS (Figure 3b) is slightly lower than for MS (see Figure 3a) and F samples, indicating good barrier properties for the back reaction (holes trying to cross the BL).

Figure 3 shows, at potentials between 0.2 and 0.5 V, a visible change in the anodic current curve for MS with respect to OS. Considering that the oxidation process of the sputtered Ti metal was not fully completed during the sintering in air at 450 °C for 30 min, the application of a positive potential may have oxidized part of the metallic film.

3.2. Performance of DSCs. Figure 4 presents the characteristic $j-V$ curves of DSCs with the different BLs under standard global AM 1.5 conditions and 1 sun light intensity (1000 W·m^{-2}). Three samples of each type were prepared to ensure the consistency of the results.

Characteristic parameters such as open-circuit voltage (V_{oc}), short-circuit photocurrent density (j_{sc}), fill factor (FF), and efficiency (η), calculated from the results shown in Figure 4, are summarized in Table 2. The changes observed in the performance of the solar cells are mostly due to the variations observed in j_{sc}, with some contribution from FF, while V_{oc} remains almost unchanged for all samples. The first noticeable effect, for the cells with BLs, is that, in general, their overall efficiency decreases when the thickness of the BL increases. Therefore, despite the initial rise in the photocurrent obtained after the deposition of a thin BL, the thicker the film, the lower

dx.doi.org/10.1021/jp301694r | J. Phys. Chem. C 2012, 116, 12415−12421

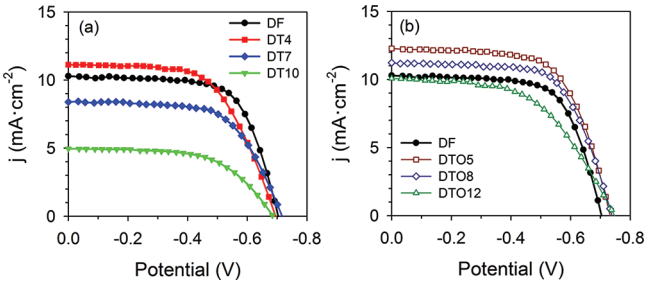

Figure 4. $j-V$ curves of DSCs, with and without BLs, under AM 1.5, 1 sun illumination conditions. The BLs were obtained from metal (a) and oxide (b) sputtering targets.

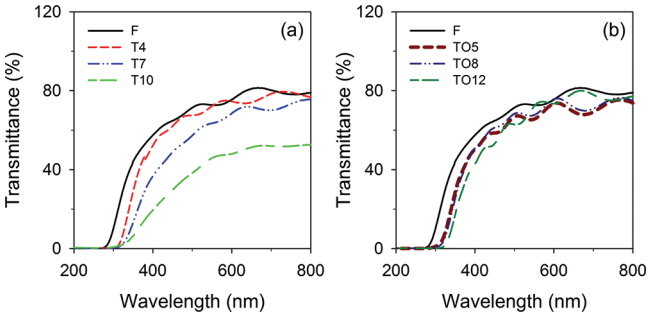

Figure 5. UV−vis transmittance spectra, as a function of wavelength, for the bare and BL-coated FTO: MS (a) and OS (b).

the j_{sc} (see Figure 4). Moreover, samples with BLs made from metallic sputtered films present lower performance than their oxide counterparts (Figure4b) and the uncoated reference.

The behavior of the BLs made from metallic films may be understood by looking at Figure 5a, where the UV−vis spectra of the FTO with BLs are compared with the transmittance of the uncoated FTO. As the BL thickness increases, the transmittance of the film decreases, and consequently, the photocurrent drops. These optical measurements suggest that samples DT7 and DT10 contain larger amounts of metallic titanium that have not been oxidized during the thermal processing. The transmittance of sample DT4 suggests that for this sample the thermal treatment was enough to fully oxidize the metallic layer. However, for the oxide films, it is not possible to attribute the decrease in photocurrent to differences in transmittance of the BL because all of the samples present very similar optical properties (Figure 5b).

3.3. Impedance Spectroscopy Analysis of DSCs. In a previous article by our group, involving the analyses of a large number of samples, we observed a good reproducibility in cell performance.[26] For that work, we used the same TiO_2 paste, electrolyte, and assembling procedure and observed that the amount of dye adsorption was the same for all DSCs. Therefore, since we adopted identical experimental conditions in the present work, we consider that all of the effects in the performance of the DSCs reported herein can be attributed to the presence of the BLs.

By using impedance spectroscopy, effects such as the competition between electron interception (normally by I_3^- ions) and diffusion to the current collector can be, under the appropriate conditions, distinguished according to the spectral shapes of the impedance response as a function of frequency.[10,23,27] As the oxide series presented better performance, the following discussion will be primarily focused on the IS analysis of these samples. The analysis of the MS series was conducted in a similar way (see Figures S2 and S3 in the Supporting Information), and the more relevant results are discussed at the end of this section.

Figure 6 shows the impedance of the DSC samples assembled with bare FTO and OS as BLs under 1 sun illumination at −0.75 V, a potential near V_{oc}.

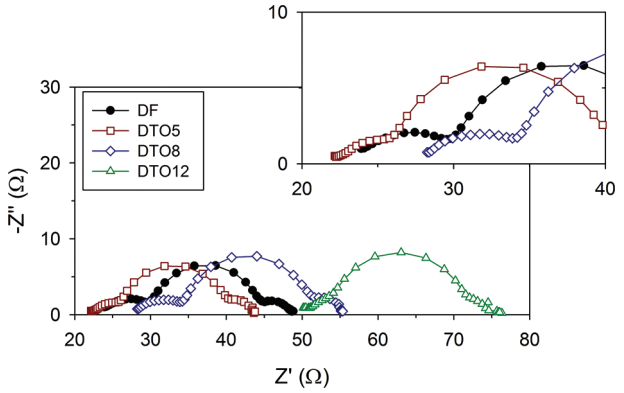

Figure 6. Impedance spectra of DSCs at a potential close to V_{oc} (−0.75 V) measured under 1 sun illumination for the samples with and without BLs. The thicker the BL, the larger the displacement of the impedance spectrum to the right side due to the R_S contribution.

The high frequency arc is due to the resistance and capacitance at the platinum counter electrode, the low frequency arc is attributed to the impedance of diffusion of redox species in the electrolyte, and the intermediate frequency arc is the recombination resistance (R_{rec}) associated to electron recombination at the interface, combined with the chemical capacitance (C_μ) of electrons in TiO_2. Finally, the displacement of the arc is attributed to the contribution to the total series resistance (R_{series}) of wiring, FTO, and BLs (R_S). As shown in Figure 6 (and also in the Supporting Information), this displacement due to R_S increases with the thickness of the BL.

The short circuit photocurrent, for a given dye, may be influenced by: (i) its ability to inject charge on the semiconductor; (ii) the speed with which it is regenerated, and (iii) the efficiency with which the photogenerated charge is

Table 2. Performance Parameters of DSCs Tested under AM 1.5, 1 Sun Illumination Conditions

	reference	metallic series			oxide series		
parameter	DF	DT4	DT7	DT10	DTO5	DTO8	DTO12
V_{oc} (V)	0.71	0.70	0.72	0.68	0.73	0.74	0.74
j_{sc} (mA·cm^{-2})	10.29	11.13	8.39	4.96	12.27	11.23	10.07
FF	0.67	0.59	0.62	0.59	0.65	0.66	0.53
η (%)	4.83	4.57	3.75	1.99	5.81	5.42	3.96
DSC area (cm^2)	0.20	0.25	0.33	0.30	0.23	0.22	0.22

dx.doi.org/10.1021/jp301694r | J. Phys. Chem. C 2012, 116, 12415−12421

transferred into the collecting electrode. While the second aspect (ii) may not be influenced by the existence of the BL, through impedance spectroscopy we may analyze the other two processes.

Injection of charge into the TiO_2 may be modulated by the position of its conduction band edge, E_c. A good way to study displacements in E_c is to compare the chemical capacitance of the different samples.[7,28] The values of C_μ are given by:[29]

$$C_\mu = C_0 \exp\left[\frac{E_{Fn} - E_c}{k_B T_0}\right] \quad (1)$$

where C_0 is a constant depending on semiconductor properties and geometry, k_B is the Boltzmann constant, T_0 is a parameter with temperature units that determines the depth of the trap distribution (T_0 = 800−1200 K),[23] and E_{Fn} is the titania quasi-Fermi-level which correlates with the potential in the film (V_F) through $qV_F = E_{redox} - E_{Fn}$, with E_{redox} being the equilibrium energy of the redox species or, in other words, the position of the Fermi level of the holes in the electrolyte.

On the other hand, for a certain range of potentials, the charge transfer resistance arising at the porous nanostructured electrode in contact with liquid electrolyte may be described by using a recombination resistance as:[8]

$$R_{rec} = R_0 \exp\left[\beta\frac{E_{redox} - E_{Fn}}{k_B T}\right] \quad (2)$$

in which R_0 is a constant indicating the onset of recombination, β is the transfer factor governing the recombination, and T is the temperature.

Figure 7 shows the capacitance and recombination resistance plotted versus potential drop at the sensitized electrode. Note

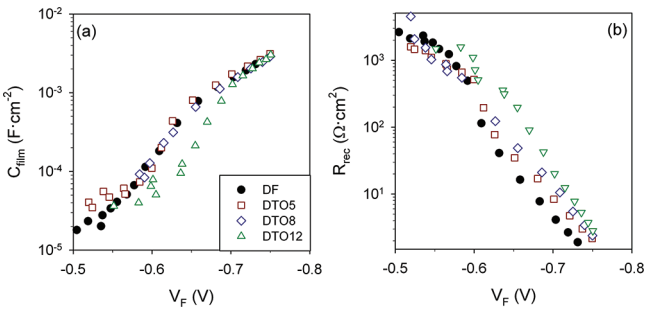

Figure 7. Electrode capacitance (a) and recombination resistance (b) obtained by impedance spectroscopy of DSCs under 1 sun illumination.

that V_F is obtained after correcting the applied potential (V_{app}) for the drop at total series resistance (V_s) collected from impedance spectroscopy data.[7] The values of these parameters can be determined from $V_F = V_{app} - V_s$ with $V_s = (j/(j_{sc} - j))\int_{jsc}^{j} R_{series}\, dj$ and $R_{series} = R_{Pt} + R_S + R_d$.[13,27]

Figure 7a represents the capacitance of the working electrodes for the full range of potentials measured. Note that the correction of the potential drop at the series resistance constrains the variation of the potential in the TiO_2 film to the range from −0.5 to −0.8 V. At the lower potentials the capacitance is dominated by the Helmholtz layer at the FTO (+ BL) in contact with the electrolyte which is uncovered by the colloids. Similarly to the three electrode measurements (Section 3.1), in the solar cells with BLs, the capacitance associated to the BL/electrolyte interface is larger than in the case of bare FTO. At intermediate and high potentials, we can observe the characteristic exponential rise of C_μ, indicating that we are charging the semiconductor colloidal matrix. Comparing the chemical capacitance of the different samples, one can see that the conduction band in the semiconductor nanoparticles does not present a relevant shift. Therefore, the charge injection is not limited by an energy mismatch between E_c in TiO_2 and LUMO in the dye.[11,30] In the full range of potentials applied, we were not able to distinguish the transport resistance. This means that the transport resistance is much smaller than recombination resistance and thus the diffusion length is large enough to transport electrons through the whole film thickness.[31]

Several papers claim that the application of a BL over FTO prevents the loss of photogenerated current through a FTO/electrolyte recombination.[14,16,32] Other authors claim that the BL improves the connection of the nanoparticles to the collecting electrode, improving in this way the charge collection efficiency.[16,33,34] However, the effectiveness of the BL on the performance of the cell is negligible for dyes such N719[16] and lost if the BL is too thick.[21]

We will use the measurements under 1 sun illumination, which reproduce real operation conditions, to find the origin of the changes in performance found for our cells. Recombination resistance at the lowest V_F is very close for all of the cases and larger than 1 kΩ·cm^2 (see Figure 7b). These values of V_F correspond to short circuit conditions (see Figure S3 in the Supporting Information), where recombination from the BL is believed to dominate. Therefore here, the differences found for the photocurrent may not be attributed to changes in the recombination losses produced by the addition of the BL.

Although IS measurements could not provide direct evidence of the improved contact between colloids and the FTO, this enhanced connection may be estimated indirectly. By plotting the series resistance of the film versus film thickness (Figure 8a), it is possible to observe that while the series resistance of

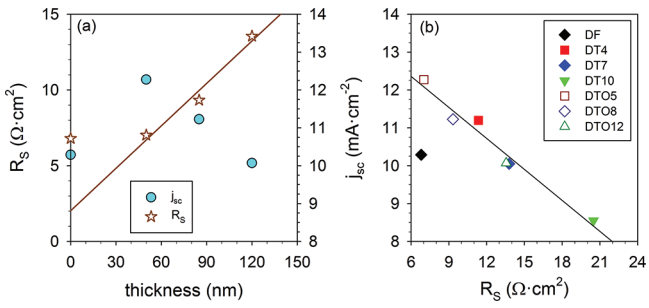

Figure 8. (a) Series resistance (left axis) and photocurrent (right axis) of the solar cells as a function of the thickness of the BL deposited by oxide sputtering. (b) Photocurrent density plotted against the series resistance for all of the samples tested in this work. Photocurrent data for the metallic samples have been corrected taking into account the losses due to the lower transmittance of the BL.

the films with BL increases linearly with the thickness, the R_S of the uncoated sample does not follow this tendency. If we assume that the contact resistance between FTO and BL and between BL and the colloidal matrix is zero (ohmic contact), we may attribute the 4.8 Ω·cm^2 difference between the axis intercept of the tendency line of the BL samples and the R_S of FTO sample to the presence of a nonohmic contact. A similar

dx.doi.org/10.1021/jp301694r | J. Phys. Chem. C 2012, 116, 12415−12421

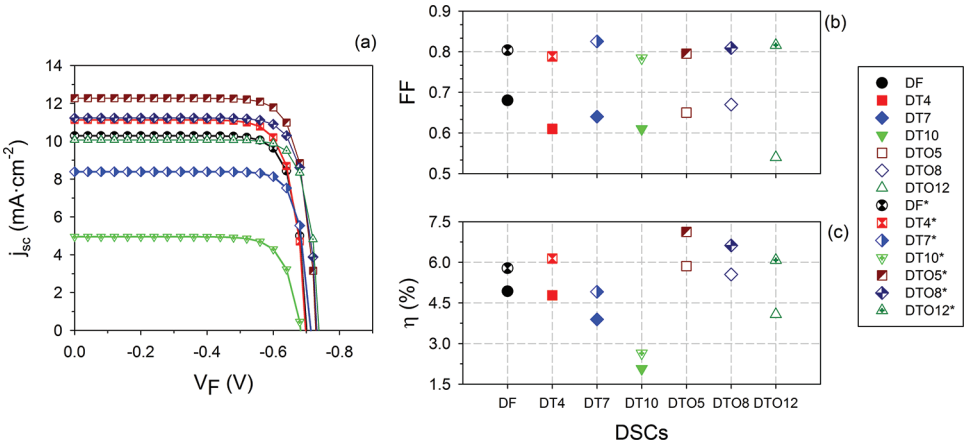

Figure 9. (a) $j-V$ curves corrected for the effect of total series resistance; FF (b) and efficiency (c) for the devices with and without BL. The symbol (*) in the legend indicates the values of efficiency and fill factor after subtracting the effect of series resistance.

result has been recently found by Wang and co-workers.[35] This poor contact between FTO and the TiO_2 nanoparticles seems to be associated to the lower j_{sc} found for this sample with respect to the thin BL samples.

The slope of the resistance in Figure 8 presents the resistivity of the TiO_2 BL, from which we may obtain the conductivity, $\sigma = 1/\rho = 1.1 \times 10^{-6}$ S·cm^{-1}, an intermediate value in the range obtained by Abayev.[36] Considering a value of $\mu = 2.3 \times 10^{-4}$ cm^2·V^{-1}·s^{-1} for the mobility of free electrons in the TiO_2,[36] the estimated free electron density in the BL is 3×10^{16} cm^{-3} (a value near the number of photons absorbed by N719 in 1 s at 1 sun and 2 orders of magnitude larger than native bulk TiO_2), compatible with the assumption of the presence of a notable electron density made previously. This result has to be carefully considered, having in mind the large dispersion of values for μ reported in the literature which ranges between 10^{-5} and 1 cm^2·V^{-1}·s^{-1}.[37,38]

The origin of the reduction in the j_{sc} with increasing film thickness, for both MS and OS shown in Figure 8a, still remains unclear. The photocurrent decrease due to the lower light transmission of the MS BL may be estimated by integrating transmittance (T_{BL}) data times spectral irradiance (I) and dye absorbance (A) with respect to wavelength.

$$j_{sc,max} = \int T_{BL}(\lambda)[1 - 10^{-A(\lambda)}]I(\lambda)d\lambda \quad (3)$$

This leads to a correction of the photocurrent decrease due to the light transmission losses occurring in the metallic BLs, of 20% for sample DT7 and of 72% for DT10 with respect to the values obtained for DT4. Once correcting the photocurrent from BL transmittance, the values obtained were used in Figure 8b for comparison. In this figure, we observe that, with exception of the sample without BL, j_{sc} decreases linearly as the series resistance increases. A similar result was also observed by Zaban's group when using aged counter-electrodes with increasing R_{Pt}.[39] In standard solar cell models, the effect of series resistance may not affect the photocurrent except for extreme cases (very large values of series resistance and/or photocurrent), but this does not apply here.[12] In fact, if an additional series resistance is connected to the DSC, the photocurrent remains unchanged, as long as this resistance is not too large. As expected in this case, only the FF is affected by the addition of this resistance.[12,13,40,41] The dependence of j_{sc} on the R_{series} shown here indicates that, as in the paper by Zaban, the increment of this resistance has a critical effect on performance that has to be accounted for in solar cell design. In our case, the thicker BLs act as barrier for the optimal collection of photogenerated electrons.

The other parameter that influences the performance of the solar cell is the recombination resistance. The charge losses of the photoelectrons injected into the mesoporous TiO_2 with the holes present in the redox carrier is the main factor determining both the photopotential and the maximum performance of the cell.[9,13,40,41] Therefore, here the origin of the lower V_{oc} found for the DSC made from bare FTO is due to its lower R_{rec}, in the region near V_{oc} (Figure 7b). The same applies to the small rise in V_{oc} found for both DTO8 and DTO12 with respect to DTO5, despite the higher j_{sc}.

Finally, the maximum attainable FF is reduced by the effect of the series resistance.[12,13,40,41] Figure 9 shows the $j-V$ curves from Figure 4 corrected from the effect of total series resistance. The increasing values of this resistance associated to the thicker BL produce a decay in the FF and, consequently, in the overall performance of the cell. Without the series resistance, the FF for all of the samples would increase to values of around 0.8, and cell efficiencies would rise approximately 25% for DTO5 and DTO8 and ~50% for DTO12. In the case of DT4 and DTO5, the lower FF is associated to the higher photocurrent that producing larger potential drops in total series resistance.

4. CONCLUSIONS

The application of sputtered TiO_2 BLs between FTO and mesoporous TiO_2 produced improvements in the conversion efficiency up to ~25% with respect to a reference cell made without these layers. The main factor producing the rise in efficiency was the larger photocurrent obtained when using thin BLs. After discarding conduction band shifts and charge collection limitations associated to diffusion length, the origin of this improvement was attributed to a better contact between the coated FTO substrate and the TiO_2 film. Other minor contributions to solar cell performance have been attributed to changes in series resistance associated to BL thickness which modify the fill factor.

A remarkable result was the linear dependence of photocurrent on BL thickness associated with the internal series resistance of the cell. This result suggests that thick BLs generate an electron barrier that reduces the charge collection

efficiency. Therefore, the advantage gained by using BLs, due to improved contact, is lost if the thickness of these layers is too large.

■ ASSOCIATED CONTENT

Supporting Information

Cyclic voltammetry of the BLs in semilogarithmic scale, impedance spectra, and data of DSC samples with BL made from metallic depositions and the variation of photocurrent with BL thickness. This material is available free of charge via the Internet at http://pubs.acs.org.

■ AUTHOR INFORMATION

Corresponding Author

*Tel.: +34964 387537. E-mail: fran.fabregat@fca.uji.es (F.F.S.) and marcgoes@iq.unesp.br (M.S.G.).

Notes

The authors declare no competing financial interest.

■ ACKNOWLEDGMENTS

This work was carried out with the financial support of FAPESP, CAPES, and CNPq (Brasil). M.S.G. thanks FAPESP (2009/14713-3) and CAPES (BEX3135/10-1) for the post-doctoral fellowship. The Spanish team acknowledges the support given by Generalitat Valenciana under project PROMETEO/2009/058 and Ministerio de Ciencia e Innovación under projects PHB-2008-040-PC, MAT2010-19827, and HOPE—CSD2007-00007.

■ REFERENCES

(1) O'Regan, B.; Grätzel, M. *Nature* **1991**, *353*, 737.
(2) Barbé, C. J.; Arendse, F.; Comte, P.; Jirousek, M.; Lenzmann, F.; Shklover, V.; Grätzel, M. *J. Am. Ceram. Soc.* **1997**, *80*, 3157.
(3) de Almeida, P.; van Deelen, J.; Catry, C.; Sneyers, H.; Pataki, T.; Andriessen, R.; Van Roost, C.; Kroon, J. M. *Appl. Phys. A: Mater. Sci. Process.* **2004**, *79*, 1819.
(4) Cao, Y.; Bai, Y.; Yu, Q.; Cheng, Y.; Liu, S.; Shi, D.; Gao, F.; Wang, P. *J. Phys. Chem. C* **2009**, *113*, 6290.
(5) Yu, Q.; Wang, Y.; Yi, Z.; Zu, N.; Zhang, J.; Zhang, M.; Wang, P. *ACS Nano* **2010**, *4*, 6032.
(6) Bessho, T.; Zakeeruddin, S. M.; Yeh, C.-Y.; Diau, E. W.-G.; Grätzel, M. *Angew. Chem., Int. Ed.* **2010**, *49*, 6646.
(7) Mora-Seró, I.; Bisquert, J. *J. Phys. Chem. Lett.* **2010**, *1*, 3046.
(8) Fabregat-Santiago, F.; Bisquert, J.; Garcia-Belmonte, G.; Boschloo, G.; Hagfeldt, A. *Sol. Energy Mater. Sol. Cells* **2005**, *87*, 117.
(9) Fabregat-Santiago, F.; Bisquert, J.; Palomares, E.; Otero, L.; Kuang, D.; Zakeeruddin, S. M.; Gratzel, M. *J. Phys. Chem. C* **2007**, *111*, 6550.
(10) Lee, B.; Hwang, D.-K.; Guo, P.; Ho, S.-T.; Buchholtz, D. B.; Wang, C.-Y.; Chang, R. P. H. *J. Phys. Chem. B* **2010**, *114*, 14582.
(11) Barea, E. M.; Ortiz, J.; Paya, F. J.; Fernandez-Lazaro, F.; Fabregat-Santiago, F.; Sastre-Santos, A.; Bisquert, J. *Energy Environ. Sci.* **2010**, *3*, 1985.
(12) Sze, S. M. *Physics of Semiconductor Devices*, 2nd ed.; John Wiley and Sons: New York, 1981.
(13) Fabregat-Santiago, F.; Garcia-Belmonte, G.; Mora-Sero, I.; Bisquert, J. *Phys. Chem. Chem. Phys.* **2011**, *13*, 9083.
(14) Cameron, P. J.; Peter, L. M. *J. Phys. Chem. B* **2003**, *107*, 14394.
(15) Cameron, P. J.; Peter, L. M. *J. Phys. Chem. B* **2005**, *109*, 7392.
(16) Ito, S.; Liska, P.; Comte, P.; Charvet, R.; Pechy, P.; Bach, U.; Schmidt-Mende, L.; Zakeeruddin, S. M.; Kay, A.; Nazeeruddin, M. K.; Gratzel, M. *Chem. Commun.* **2005**, 4351.
(17) Kay, A.; Grätzel, M. *Chem. Mater.* **2002**, *14*, 2930.
(18) Menzies, D. B.; Bourgeois, L.; Cheng, Y. B.; Simon, G. P.; Brack, N.; Spiccia, L. *Surf. Coat. Technol.* **2005**, *198*, 118.
(19) Li, T. C.; Góes, M. S.; Fabregat-Santiago, F.; Bisquert, J.; Bueno, P. R.; Prasittichai, C.; Hupp, J. T.; Marks, T. J. *J. Phys. Chem. C* **2009**, *113*, 18385.
(20) Patrocínio, A. O. T.; Paterno, L. G.; Murakami Iha, N. Y. *J. Photochem. Photobiol., A* **2009**, *205*, 23.
(21) Yoo, B.; Kim, K.-J.; Bang, S.-Y.; Ko, M. J.; Kim, K.; Park, N.-G. *J. Electroanal. Chem.* **2010**, *638*, 161.
(22) Boschloo, G.; Hagfeldt, A. *Acc. Chem. Res.* **2009**, *42*, 1819.
(23) Wang, Q.; Ito, S.; Gratzel, M.; Fabregat-Santiago, F.; Mora-Sero, I.; Bisquert, J.; Bessho, T.; Imai, H. *J. Phys. Chem. B* **2006**, *110*, 25210.
(24) He, C.; Zheng, Z.; Tang, H.; Zhao, L.; Lu, F. *J. Phys. Chem. C* **2009**, *113*, 10322.
(25) Fabregat-Santiago, F.; Garcia-Belmonte, G.; Bisquert, J.; Zaban, A.; Salvador, P. *J. Phys. Chem. B* **2002**, *106*, 334.
(26) Muniz, E. C.; Góes, M. S.; Silva, J. J.; Varela, J. A.; Joanni, E.; Parra, R.; Bueno, P. R. *Ceram. Int.* **2011**, *37*, 1017.
(27) Wang, Q.; Moser, J.-E.; Gratzel, M. *J. Phys. Chem. B* **2005**, *109*, 14945.
(28) Bisquert, J.; Cahen, D.; Hodes, G.; Ruhle, S.; Zaban, A. *J. Phys. Chem. B* **2004**, *108*, 8106.
(29) Bisquert, J. *Phys. Chem. Chem. Phys.* **2003**, *5*, 5360.
(30) Liu, Y.; Hagfeldt, A.; Xiao, X.-R.; Lindquist, S.-E. *Sol. Energy Mater. Sol. Cells* **1998**, *55*, 267.
(31) Bisquert, J. *J. Phys. Chem. B* **2002**, *106*, 325.
(32) Hattori, R.; Goto, H. *Thin Solid Films* **2007**, *515*, 8045.
(33) Zeng, L.-Y.; Dai, S.-Y.; Wang, K.-J.; Pan, X.; Shi, C.-W.; Guo, L. *Chin. Phys. Lett.* **2004**, *21*, 1835.
(34) Xia, J.; Masaki, N.; Jiang, K.; Yanagida, S. *J. Phys. Chem. B* **2006**, *110*, 25222.
(35) Jennings, J. R.; Liu, Y.; Safari-Alamuti, F.; Wang, Q. *J. Phys. Chem. C* **2012**, *116*, 1556−1562.
(36) Abayev, I.; Zaban, A.; Fabregat-Santiago, F.; Bisquert, J. *Phys. Status Solidi A* **2003**, *196*, R4.
(37) Dittrich, T.; Lebedev, E. A.; Weidmann, J. *Phys. Status Solidi A* **1998**, *165*, R5.
(38) Forro, L.; Chauvet, O.; Emin, D.; Zuppiroli, L.; Berger, H.; Lévy, F. *J. Appl. Phys.* **1994**, *75*, 633.
(39) Hod, I.; Tachan, Z.; Shalom, M.; Zaban, A. *J. Phys. Chem. Lett.* **2011**, *2*, 1032.
(40) Adachi, M.; Murata, Y.; Takao, J.; Jiu, J.; Sakamoto, M.; Wang, F. *J. Am. Chem. Soc.* **2004**, *126*, 14943.
(41) Nakade, S.; Saito, Y.; Kubo, W.; Kitamura, T.; Wada, Y.; Yanagida, S. *J. Phys. Chem. B* **2003**, *107*, 8607.